Colloid Polym Sci (2007) 285:1423–1431
DOI 10.1007/s00396-007-1698-5

ORIGINAL CONTRIBUTION

The self-organization properties of *n*-dodecylammonium α-glutamate/*n*-$C_5H_{11}OH$/water system

Yongsheng Wang · Rong Guo · Xia Guo

Received: 6 February 2007 / Accepted: 9 May 2007 / Published online: 13 July 2007

Abstract A biocompatible surfactant-*n*-dodecylammonium α-glutamate (GDA) with biodegradable and biocompatible properties was synthesized, and the phase behavior and the structural properties of GDA/*n*-pentanol/water system was studied by small-angle X-ray diffraction, electron spin resonance, and freeze-fracture transmission electron microscopy (FF-TEM). In the ternary phase diagram of GDA/*n*-pentanol/water system, there exist three isotropic regions—O/W, bicontinuous, and W/O structures, and two anisotropic regions—hexagonal liquid crystal (HEX), and lamellar liquid crystal (LLC) regions. UV irradiation causes the decrease in the interlayer space, *d*, of lamellar liquid crystal and in the radius, *r*, of column aggregates of hexagonal liquid crystal, but it has little effect on the structure of O/W and W/O microemulsions.

Keywords GDA · Small-angle X-ray diffraction · Microemulsions · Lyotropic liquid crystal · UV irradiation

Introduction

Surfactants have been extensively used in simulating biomembrane [1–5]. J.H. Fendler [6] suggests that micelles, microemulsions, lyotropic liquid crystal, etc., which are formed by surfactants, can be used as biomembranes for drug delivery and drug extraction [7–10]. However, some problems arise due to the nonbiocompatibility and environmental pollution of traditional surfactants used [11–14]. Therefore, studies about biocompatible surfactants are of great interest [15]. Amino-acid-based surfactants are one kind of biocompatible surfactants [16–18]. Currently, the biodegradability, phase behavior, self-assembly properties, and biocompatibility [19–21] of arginine-based surfactants have been studied extensively. The salt of glutamic acid cannot only be used in flavorings, but can also be used as a medicine that can cure neurasthenic, hypomnesis, etc. [22]. Moreover, glutamic-acid-based surfactants have considerable application prospects in such fields as drug delivery, drug package, and enzyme reaction [18]. Thus, a glutamic-acid-based surfactant-*n*-dodecylammonium α-glutamate (GDA) was synthesized. GDA not only has general characteristics of normal ionic surfactants, but also has carboxyl and amidocyanogen in the molecule, which make GDA show different structures with different pH and furthermore affect the structures of organized assemblies formed by GDA, and in this paper, the structural properties of organized assemblies formed by GDA were investigated by phase diagram, small angle X-ray, electron spin resonance (ESR), and freeze-fracture transmission electron microscopy (FF-TEM).

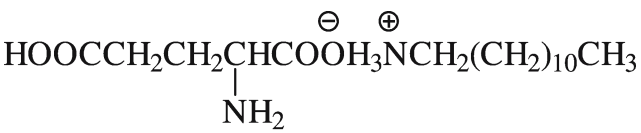

GDA

Usually, the changes of the structure of cell membranes can cause some diseases [23]. Such as, by comparing a cancer cell with a normal one, the fluidness of cancer cell membrane increases, and the arrangement of

Y. Wang · R. Guo (✉) · X. Guo
School of Chemistry and Chemical Engineering,
Yangzhou University,
Yangzhou 225002, People's Republic of China
e-mail: guorong@yzu.edu.cn

membrane molecules becomes irregular [24, 25]. Hence, developing various novel therapies in improving the structure of cell membranes becomes more and more interesting, especially, UV therapy attracted great attention due to its high convenience and lower side effect [26]. As described above, the molecular organized assemblies formed by surfactants, especially the biocompatible self-assemblies with photosensitivity are ideal model biomembranes. Therefore, the organized assemblies formed by biocompatible GDA with photosensitivity were chosen to simulate the effect of UV irradiation on the structure of cell membranes. It is found that the UV irradiation can improve the regularity of molecule arrangement of model membranes, which may promise a potential application in cancer therapy.

Experimental section

Materials and methods

L-Glutamic acid was a biochemistry reagent and was obtained from Shanghai Biochemistry Reagent, China. The *n*-pentanol was from Aldrich, 5-doxyl stearic acid (5-DXSA) and dodecylamine from Sigma. The water used was distilled twice.

The *n*-dodecylammonium α-glutamate (GDA) was synthesized according to the reference [18]. m.p.: 138.5± 0.5 ° C, $\delta^{1}_{\text{H-NMR}}$ (ppm, solvent: D_2O): 0.830 (t, $-CH_3$, 3H), 1.245 (*m*, $-(CH_2)_9-$, 18H), 1.623 (*m*, $-CH_2-$, 2H), 2.060 (*m*, $-CH_2-$, 2H), 2.300 (*m*, $-CH_2-$, 2H), 2.911 (*t*, $-CH_2-$, 2H), 3.715 (*t*, CH,1H).

Determination of partial phase diagram

The isotropic regions of GDA/*n*-$C_5H_{11}OH/H_2O$ system were determined by observing the change point from clarity to cloudiness when GDA was added to the samples with different weight ratios of *n*-$C_5H_{11}OH/H_2O$, or when *n*-$C_5H_{11}OH$ was titrated into the samples with different weight ratios of GDA/H_2O. Microemulsion samples were placed in a thermostat at 25±0.1 °C for at least 2 h for phase equilibrium; liquid crystal samples were placed in a thermostat at 25±0.1 °C for at least 1 day for phase equilibrium. The phase boundaries of liquid crystals were determined with a Leica DM LM/P polarizing microscope (Leica, Germany), and the precision was limited to ±0.5%.

UV-irradiation of GDA/*n*-$C_5H_{11}OH/H_2O$ system

GDA/*n*-$C_5H_{11}OH/H_2O$ system, placed in a quartz test tube, was irradiated by a 125-W high-pressure mercury lamp (Shanghai Yaming Lamp, China). The distance between the mercury lamp and the quartz test tube was kept at 5.0 cm.

Measurement of gas chromatography spectra

The lamellar liquid crystal of GDA/*n*-$C_5H_{11}OH/H_2O$ system was diluted to form an isotropic solution with water, and then the resulting sample was used for gas chromatography measurement (GC-14B, Shimadzu, Japan). The column was DB-17 capillary column. The pressure of nitrogen was 0.5 MPa. The temperatures of the injector, detector, and oven were 150, 190, and 190 °C, respectively.

Measurement of images

The images of the samples were observed by transmission electronic microscopy (Tecnai 12, Philips Apparatus, Netherlands) after being freeze-fractured (BAF 400 D, Balzers, Liechtenstein).

Measurement of fluorescence life time for excited GDA molecules

The fluorescence life time for excited GDA molecules was determined with a time resolved fluorescence spectrometer (model: FLS920, Edinburgh instruments, UK).

Measurement of small-angle X-ray diffraction

Small-angle X-ray diffraction measurements were obtained by using a D8 Advance X-ray diffractometer (Bruker, Germany) with a Ni filter and Cu radiation (λ=0.1542 nm). The tube voltage was 50 kV and tube current was 180 mA.

Determination of diffusion coefficient

A three-electrode arrangement in a conventional three-compartment cell was used. A platinum foil-working electrode, a platinum foil-auxiliary electrode, and a SCE reference electrode were used. All the solutions were deoxygenated by bubbling nitrogen. The potential was swept linearly at 50 $mV \cdot s^{-1}$ at 25±0.1 °C. Electrochemical experiments were performed using an electrochemical analyzer system with CHI 660A (Shanghai Chenhua Apparatus, China).

Measurement of ESR spectra

Added probe molecule-5-doxyl stearic acid (5-DXSA) in samples, and the concentration of 5-DXSA in each sample was 1.7×10^{-4}mol/l, and ESR measurements were performed on a Bruker A300-10/12 spectrometer with 100 KHz magnetic field modulation at room temperature (25 °C).

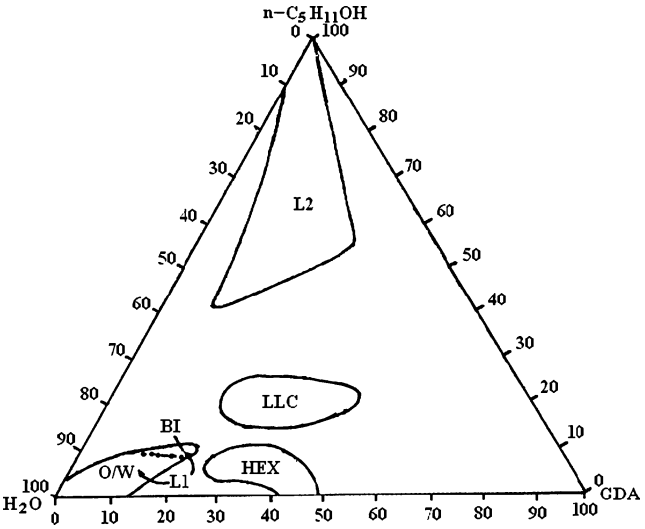

Fig. 1 Partial phase diagram of GDA/*n*-$C_5H_{11}OH/H_2O$ system at 298K. L1: consisting of O/W microemulsion and bicontinuous structure (BI) L2: W/O microemulsion region HEX: Hexagonal liquid crystal region LLC: Lamellar liquid crystal region

Results and discussion

Partial phase diagrams of GDA/*n*-$C_5H_{11}OH/H_2O$ system

Figure 1 shows the partial phase diagram of the GDA/*n*-$C_5H_{11}OH/H_2O$ system, which shows a similar phase behavior to those normal ionic surfactants ternary systems [27], in which LLC and HEX are the lamellar and hexagonal liquid crystal regions, respectively, and L2 is W/O microemulsion region. Theoretically, the isotropic region, L1, connected with water corner in the ternary phase diagram shows O/W structure, but the measurements of the diffusion coefficient show that L1 region consists of O/W (Fig. 2a and b) and bicontinuous (Fig. 2c) structure areas in the GDA/*n*-$C_5H_{11}OH/H_2O$ system, and the detailed results will be described in sections concerned. From the bottom line of the phase diagram in Fig. 1, the solubility of GDA in the water reaches 12.0 wt%. As the cmc_1 (the critical micelle concentration corresponding to the formation of spherical micelles) of GDA is 6.4×10^{-3}mol/l (about 0.2%wt) and the cmc_2 (the critical concentration corresponding to the transition from spherical to rod-like micelles) of GDA is 8.0×10^{-2}mol/l (about 2.5 wt%), respectively [28], determined by the diffusion coefficient, the structures of micelles in the O/W range should take spherical (Fig. 2a) and rod-like forms (Fig. 2b) when the GDA concentration is less and more than 2.5 wt%, respectively. Hence, some rod-like micelles gradually pack with the increase in GDA content or the decrease in water content, and finally the hexagonal liquid crystal (Fig. 2f) is formed when the content of GDA is above 12.0 wt%. It is obvious that monophase hexagonal liquid crystal appears in the range of 42.0 50.0 wt% of GDA content, and extends to lower GDA content region with increasing *n*-$C_5H_{11}OH$ content, which means that the addition of *n*-pentanol with appropriate content is beneficial to the formation of hexagonal liquid crystal. However, further addition of *n*-pentanol would cause the transformation of hexagonal liquid crystal to lamellar liquid crystal (Fig. 2e), and even that of lamellar liquid crystal to W/O microemulsions (L2 region and Fig. 2d) successively.

Structural properties of lamellar liquid crystal

The illustration of a lamellar liquid crystal structure is shown in Fig. 3a. The relationship between d_0 and d is as follows [29]:

$$d = d_0[1 + (1 - \alpha)]R \quad (1)$$

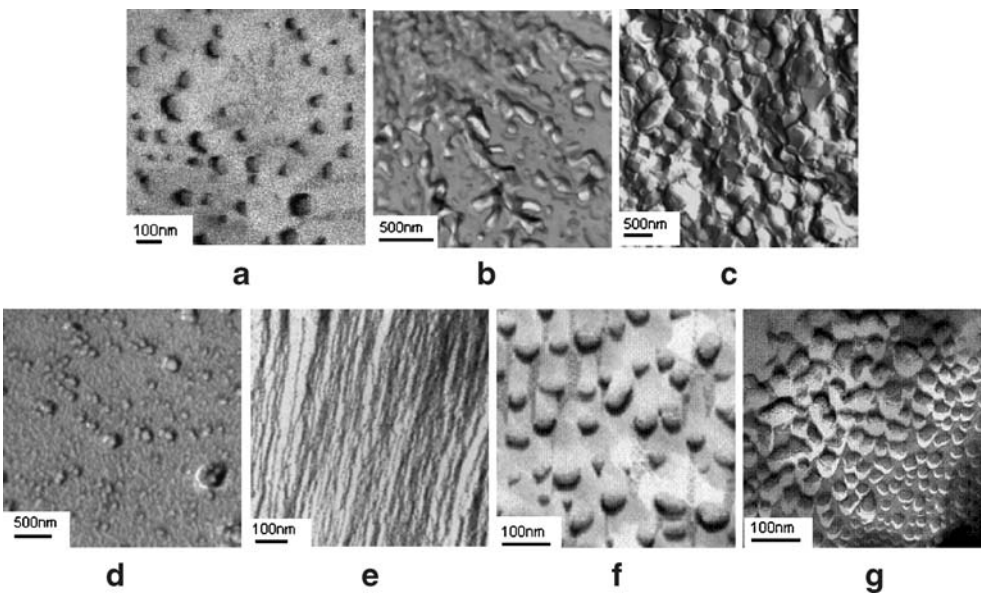

Fig. 2 Freeze-fractured TEM images of GDA/*n*-$C_5H_{11}OH/H_2O$ system. **a** GDA micelle (the content of GDA: 1.0×10^{-2}mol/l), **b** in O/W region (weight ratio: GDA/*n*-$C_5H_{11}OH/H_2O$=14.4/3.7/81.9), **c**—in BI region (weight ratio: GDA/*n*-$C_5H_{11}OH/H_2O$=18.0/10.0/72.0) **d**—in L2 region (weight ratio: GDA/*n*-$C_5H_{11}OH/H_2O$=15.7/45.0/39.3) **e**—in LLC region (weight ratio: GDA/*n*-$C_5H_{11}OH/H_2O$=23.3/20.0/56.7) **f**—in HEX region (weight ratio: GDA/*n*-$C_5H_{11}OH/H_2O$=26.6/6.7/66.7) without UV-irradiation **g**—in HEX region (weight ratio: GDA/*n*-$C_5H_{11}OH/H_2O$=26.6/6.7/66.7) after UV-irradiation 4 h

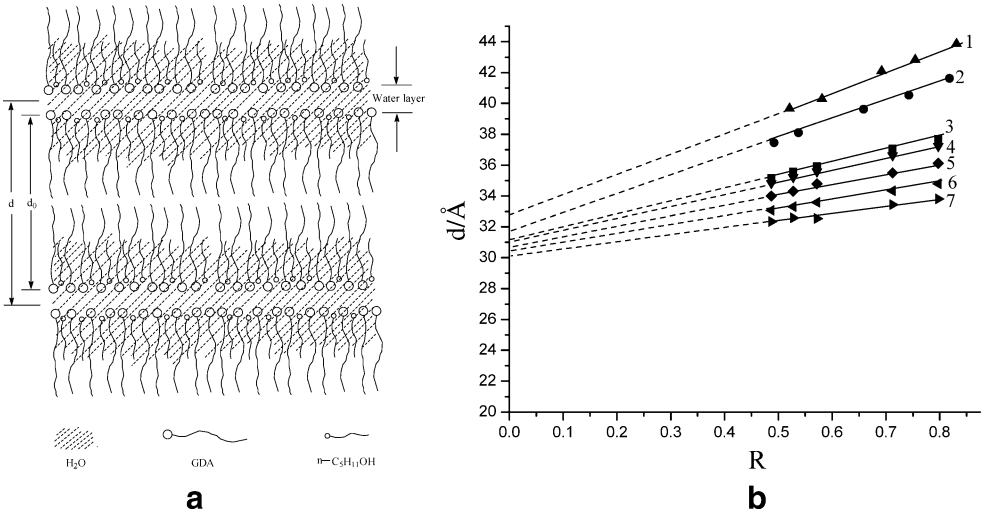

Fig. 3 Illustration of **a** lamellar liquid crystal structure, **b** the relation of d with R for lamellar liquid crystal. Weight ratio of GDA/n-$C_5H_{11}OH$: 1-63/37, 2-59/41, 3-7-53.5/46.5; the UV-irradiation time: 3–0h, 4–2 h, 5–4 h, 6–6 h, 7–8 h

in which d is the interlayer space of the lamellar liquid crystal and can be determined by small-angle X-ray diffraction, d_0 is the interlayer space without the solvent (i.e., the thickness of amphiphilic bilayer) and can be obtained by extrapolating to a zero-solvent content in Fig. 3b, R is the volume ratio of the solvent to other compositions, and α is a volume fraction of the solvent penetration from the solvent layer to the amphiphilic bilayer in the lamellar structure.

Algebraic manipulation gives a simple expression for α [30]:

$$\alpha = 1 - (\partial d/\partial R)/d_0 \quad (2)$$

Figure 3b shows the relationship of interlayer space with the volume ratio, R, in the GDA/n-$C_5H_{11}OH$/H_2O system. Figure 3b and Table 1 show the interlayer space, d, increases gradually with water content increases (i.e., R increasing) at a certain weight ratio of GDA/n-$C_5H_{11}OH$, and the interlayer spaces, d and d_0, decrease as the weight ratio of GDA/n-$C_5H_{11}OH$ is decreased. Table 1 also shows that the penetration rate of solvent, α, increases with the decreasing GDA/n-$C_5H_{11}OH$ ratio. It is obvious that the existence of more n-$C_5H_{11}OH$ molecules in the amphiphilic bilayer can (1) make the alkyl chain of GDA curled and twisted more obviously and hence, the thickness of amphiphilic bilayer, d_0, decreases, and (2) increase the solvent penetration so that the interlayer space, d, decreases.

The structure of lamellar liquid crystal is also influenced by UV-irradiation. As shown in Fig. 3b and Table 1, the thickness of amphiphilic bilayer, d_0, decreases, and the

Table 1 Parameters, d_0, r and α, for lyotropic liquid crystal with UV-irradiation time

GDA/n-$C_5H_{11}OH$ (wt:wt)	Structure	UV irradiation time (hours)	d_0 (Å)	r (Å)	α
63.0/37.0	LLC	0	32.29	–	0.57
59.0/41.0		0	31.32	–	0.60
53.5/46.5		0	31.26	–	0.74
		2	31.16	–	0.75
		4	30.86	–	0.78
		6	30.39	–	0.82
		8	29.96	–	0.84
87/13	HEX	0	–	22.50	0.42
80/20		0	–	21.08	0.44
		2	–	20.89	0.48
		4	–	20.76	0.52
		6	–	20.63	0.55
		8	–	20.33	0.57

Table 2 The parameters of various samples calculated from ESR spectra

GDA/n-$C_5H_{11}OH$/H_2O (wt:wt)	Structure	Time of UV irradiation (hours)	A_N (G)	τ_C–τ_B($\times 10^{10}$ s)
23.3/20.0/56.7	LLC	0	1.31	1.69
		1	1.42	1.89
		2	1.52	2.51
		3	1.58	3.55
		4	1.64	4.21
		5	1.66	5.28
		6	1.71	5.68
		7	1.85	6.52
		8	1.90	7.93
26.6/6.7/66.7	HEX	0	1.57	8.47
		1	1.63	10.5
		2	1.64	12.7
		3	1.68	13.1
		4	1.80	15.1
		5	1.90	17.0
		6	1.94	17.7
		7	1.99	18.4
		8	2.10	19.3

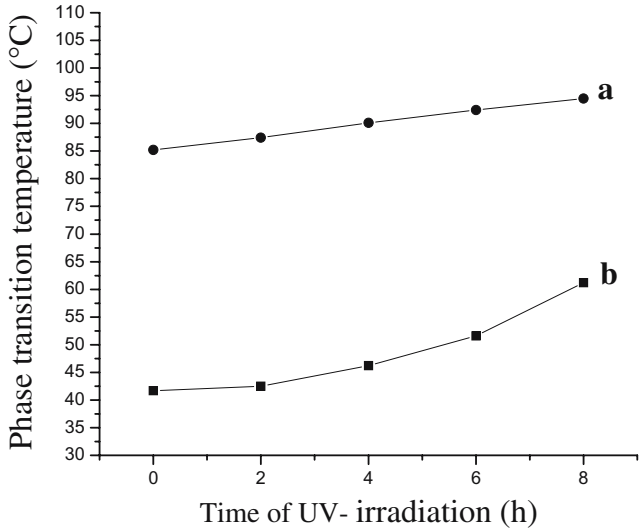

Fig. 4 Effect of UV irradiation on the temperature from lyotropic liquid crystal changing to isotropic solution **a**—LLC (weight ratio: 23.3/20.0/56.7) **b**—HEX (weight ratio: 26.6/6.7/66.7)

penetration rate, α, increases with the increasing time of UV-irradiation. After UV-irradiation, the amino groups ($-NH_2$) of GDA molecules are excited from the ground state to excited state ($-N^*H_2$), correspondly, the polarity of GDA molecules enhance [30], and the hydrogen-bond interactions between GDA molecules, and between GDA and water molecules increase, which will make more water molecules penetrate into the amphiphilic bilayer and result in the increase in the penetration rate, α (Table 1) and the decrease in interlayer space, d (Fig. 3b). Further, the increase in water penetrated into the amphiphilic bilayer of lamellar liquid crystal result in the increase in the polarity of microenvironment of GDA molecules, which causes the bending of the hydrophobic chain and decrease in the thickness of amphiphilic bilayer, d_0 (Table 1). This result also can be confirmed by ESR measurements (see support materials and Table 2). As we know [31], the probe molecules should locate in the amphiphilic bilayer of lamellar liquid crystal. Therefore, the increase in hyperfine coupling constant, A_N, with UV irradiation time (Table 2) indicate that the polarity of amphiphilic bilayer of lamellar liquid crystal increase [32]. And the increase in values of τ_C–τ_B with UV irradiation time means that the anisotropic property of the lamellar liquid crystal increases [32]. The former result indicates more water penetrates into amphiphilic bilayer from solvent layer in the lamellar liquid crystal, and the later shows the interactions between amphiphilic bilayers in the lamellar liquid crystal increase.

Gas chromatography measurement shows that UV-irradiation does not induce any chemical reaction since no new peak appears in the gas chromatography spectra for GDA/n-$C_5H_{11}OH/H_2O$ lamellar liquid crystal after UV-irradiation (Figure not shown). Furthermore, the lamellar liquid crystal that is irradiated for 8 h can restore the original state after 24 h (Table in support materials), which shows that it is a reversible process (The choice of 8 h irradiation is based on the remarkable change in the structure and polarity of liquid crystal). Thus, the probable reasons for UV irradiation causing the increase in the interactions between the amphiphilic bilayers in the lamellar liquid crystal could be: UV irradiation could make the polarity of GDA molecules increase and the hydrogen bonds between GDA and water molecules stronger than those without UV irradiation, and thus, more water penetrate into the amphiphilic bilayer, which makes both the thicknesses of solvent layer and amphiphilic bilayer decrease and the interactions between the amphiphilic bilayers in the lamellar liquid crystal increase. This result can also be confirmed by the investigation of the phase transition temperature. Curve a in Fig. 4 shows that the temperature, which corresponds to the transition of the lamellar liquid

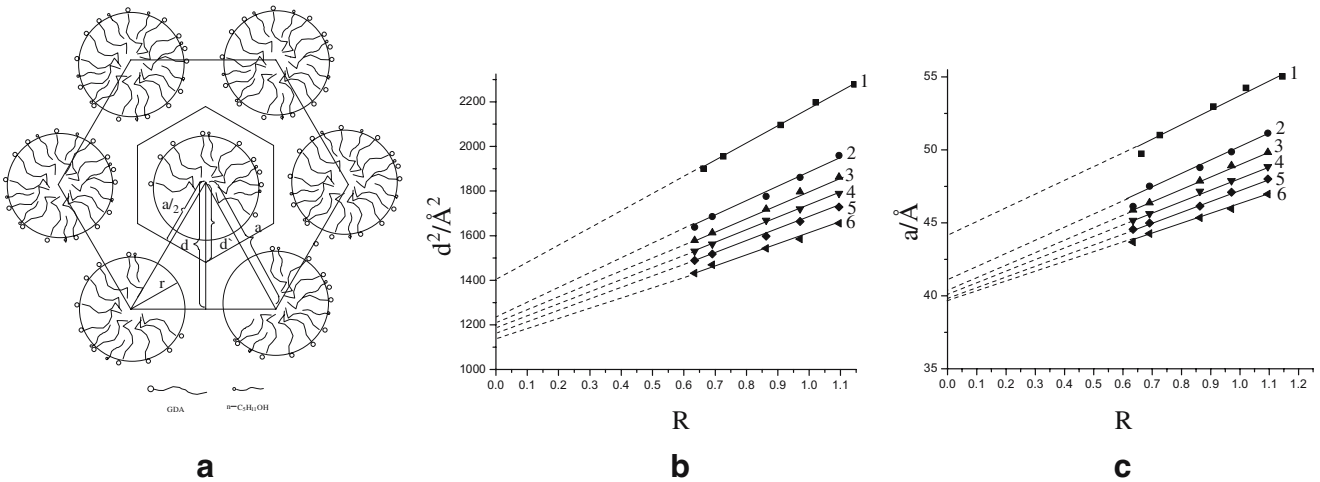

Fig. 5 Illustration of **a** hexagonal liquid crystal structure and the relation of d^2 or a with R for hexagonal liquid crystal (**b**, **c**). Weight ratio of GDA/n-$C_5H_{11}OH$: 1-87/13, 2-6-80/20; the UV irradiation time: 3–2 h, 4–4 h, 5–6 h, 6–8 h

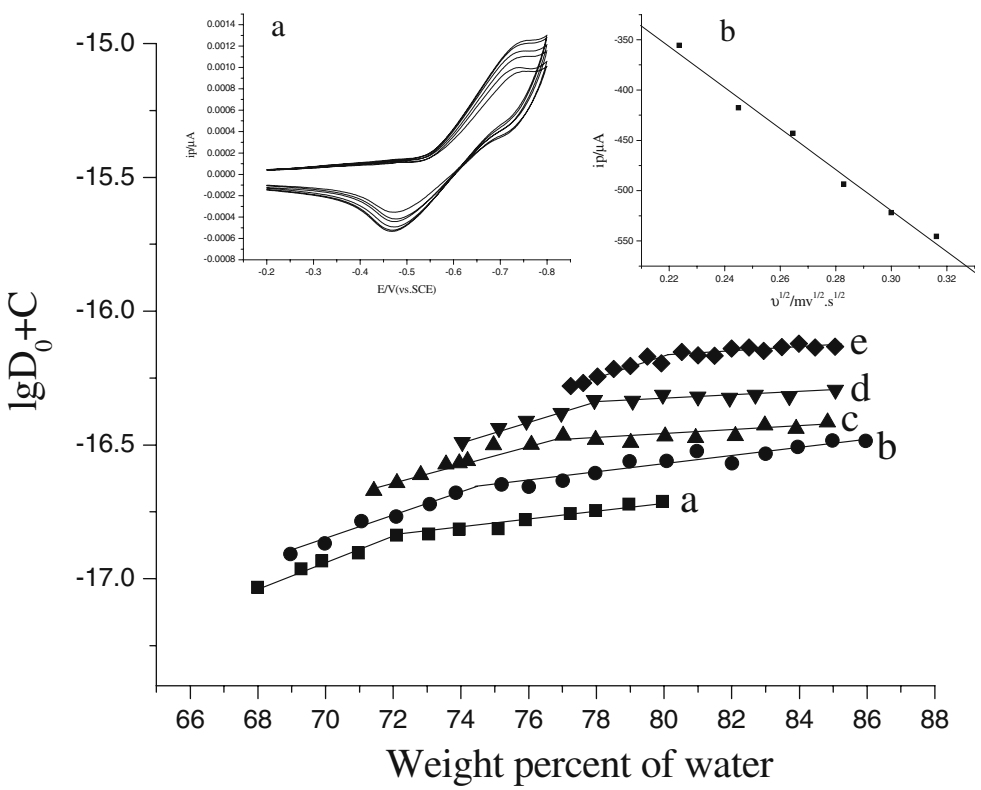

Fig. 6 Diffusion coefficient of microemulsion droplets with H_2O concentration in the different weight ratios of n-$C_5H_{11}OH$/GDA: *a*—29/71; *b*—35/65; *c*—38/62; *d*—41/59; *e*—44/56; (C=lgn$^3\beta$)

crystal to isotropic solution, increases with UV irradiation time. This phenomenon indicates that the interaction between the amphiphilic bilayers of the lamellar liquid crystal increases with UV irradiation, which is in good agreement with ESR results. It is noted that the above discussions are needed to be further verified due to the complexity of the photophysical process in the liquid crystals, such as the difficulty of the trap of excited amino groups (−N*H_2), and thus, the concerned work is in progress.

Structural properties of hexagonal liquid crystal

Figure 5a shows the structural illustration of a hexagonal liquid crystal, in which [33]

$$d = \sqrt{3}\Big/2a \tag{3}$$

Table 3 The fluorescence lifetime for GDA in GDA/n-$C_5H_{11}OH$/H_2O system

GDA/n-$C_5H_{11}OH$/H_2O (wt:wt)	Structure	τ_1(μs)	τ_2(μs)	χ^2
14.4/3.7/81.9	O/W	0.62	4.17	1.218
15.7/45.0/39.3	W/O	0.57	3.65	0.976
26.6/6.7/66.7	HEX	1.00	10.30	1.135
23.3/20.0/56.7	LLC	1.10	10.76	1.028

$$d' = a\Big/\sqrt{3} \tag{4}$$

$$d^2 = 2.72Rr^2 + 2.72r^2 \tag{5}$$

the parameter d can be determined by small angle X-ray diffraction. The radius, r, of the column aggregates of hexagonal liquid crystal and the distance, a, between column aggregates of hexagonal liquid crystal can easily be calculated from the relation of d^2 to R (Fig. 5b). The penetration of the solvent, α, from water continuous into column aggregates in the hexagonal liquid crystal, shown in Table 1, can be obtained from the equation [29, 33]:

$$\alpha = 1 - \left(\frac{\partial d^2}{\partial R}\right)\Big/ d_0^2 \tag{6}$$

It can be seen from Table 1 that the increase in n-$C_5H_{11}OH$ content in the column aggregates of hexagonal liquid crystal results in the bending of hydrophobic group in GDA molecules to a lower degree, just as in the case of lamellar liquid crystal. Thus, the radius, r, of the column aggregates decreases with the ratio of GDA/n-$C_5H_{11}OH$ decreasing (Table 1). Further, the penetration rate, α, increases, and more water molecules penetrate into the column aggregates

of hexagonal liquid crystal with the increase in n-$C_5H_{11}OH$ molecules, which result in the decrease in water content outside the column aggregates, and the decrease in distance, a, between the column aggregates (Fig. 5c).

Table 1 shows parameters, r and α, for a hexagonal liquid crystal with different UV irradiation times. The results show that the radius, r, of the column aggregates of hexagonal liquid crystal is reduced with the increase in UV-irradiation time. As discussed in the section of lamellar liquid crystal, the hyperfine coupling constant, A_N, increase with UV irradiation time, which indicates that the polarity of column aggregates of hexagonal liquid crystal increase, and the values of τ_C–τ_B also increase, which show the anisotropic property of hexagonal liquid crystal increase (Table 2) [32]. Thus, the penetration of water from the outside of the column aggregates into the inside of the column aggregates increases, and the radius, r, of the column aggregates and the distance, a, between the column aggregates of hexagonal liquid crystal decrease (Fig. 5c). These results indicate that the interactions between the column aggregates of hexagonal liquid crystal increase with UV irradiation.

The phase transition temperature of hexagonal liquid crystal can also make sure this result. Curve b in Fig. 4 shows that the temperature corresponding to the transition of the hexagonal liquid crystal to isotropic solution increases with UV-irradiation time, which also indicates the interactions between the column aggregates of hexagonal liquid crystal increase with UV-irradiation time. And the above results also revealed by the previous ESR data. Further, the above results can be illuminated directly by the illustration of the freeze-fractured image. By comparing Fig. 2g with Fig. 2f, it can be seen that the distance between two neighbor elliptical aggregates decreases after UV irradiation. However, during the process of FF-TEM measurement, it will spray Pt and carbon layers on the section of hexagonal liquid crystal accumulated by rod-like aggregates, which contributes to the larger size of the spherical section of rod-like aggregates than those from X-ray diffraction.

Structural properties of L1 and L2 regions

In L1 region in Fig. 1, the diffusion coefficient, D_0, of the GDA O/W microemulsion droplets can be determined by the cyclic voltammogram (figure A inset in Fig. 6) and calculated from the following equation at 25 °C [34]:

$$i_P = \left(2.99 \times 10^5\right) n^{3/2} \beta^{1/2} A C_0 D_0^{1/2} v^{1/2} \quad (7)$$

in which i_P is the cathodic peak current in amperes, C_0 is the solution concentration in $mol \cdot cm^{-3}$, v is the potential sweep rate in $V \cdot s^{-1}$, A is the total surface area of the Pt electrode, β is the transfer coefficient, n is the stoichometric number of electrons, and D_0 is the droplets diffusion coefficient in the solution in $cm^2 \cdot S^{-1}$.

Figure B inset in Fig. 6 shows the electrode reaction for GDA solution is a process with diffusion control, and Fig. 6 shows that the diffusion coefficients, D_0, of the isotropic droplets in L1 region increase with the water content at different weight ratios of n-$C_5H_{11}OH$/GDA, but there are several change points on the curves in which one is at 72–79% water content. By labeling the change points in L1 region in Fig. 1, L1 region can be divided into two areas: O/W and bicontinuous (BI) [33]. Comparing Fig. 2c with Fig. 2b determined by FF-TEM, the O/W microemulsion droplets show that short rod-like structure, and bicontinuous microemulsion droplets show network structure, which is consistent with the picture of bicontinuous phases described by Jahn and Strey [35].

The formation of GDA self-assemblies can result in the double exponential fluorescence decay (figures not shown) and two fluorescence life times (τ_1 and τ_2). From Table 3, it can also be seen that the fluorescence life time for excited GDA in GDA/n-$C_5H_{11}OH$/H_2O microemulsions (both O/W and W/O) is much shorter than that in GDA/n-$C_5H_{11}OH$/H_2O lytropic liquid crystal (LLC and HEX), due to the larger rigidity of the microenvironment for GDA in the latter case. Thus, UV-irradiation can remarkably change the structural properties of the lytropic liquid crystal (LLC and HEX), while it has little effect on the structural properties of the microemulsions (O/W and W/O).

Conclusions

GDA is a novel surfactant with biodegradable and biocompatible properties, which can form O/W, bicontinuous, W/O, and hexagonal and lamellar liquid crystal structures with n-pentanol as cosurfactant. Based on this, it can be used to replace normal surfactants and thus has great applications in pharmacy, cosmetic and other manufacture fields. UV irradiation can induce changes in the microstructure of lyotropic liquid crystals (LLC and HEX), and make the interactions between the amphiphilic bilayers of lamellar liquid crystal and between the column aggregates of hexagonal liquid crystal increase, indicating that UV irradiation can enhance the stability of the lyotropic liquid crystals (LLC and HEX), and can improve the molecule arrangement of model membranes, implying a potential use in phototherapy.

Acknowledgment This work was supported by the National Natural Scientific Foundation of China (No. 20633010).

Appendix

Supporting materials

Table 4 Structure parameters of X-ray diffraction for lyotropic liquid crystal with restore time after irradiating 8 h

GDA/*n*-$C_5H_{11}OH$ (wt:wt)	Structure	Restore time (hours)	d_0 (Å)	r (Å)	α
53.5/46.5	LLC	0	29.96	–	0.84
		4	30.42	–	0.83
		12	30.97	–	0.77
		24	31.27	–	0.74
80/20	HEX	0	–	20.33	0.57
		4	–	20.58	0.56
		12	–	20.99	0.47
		24	–	21.08	0.44

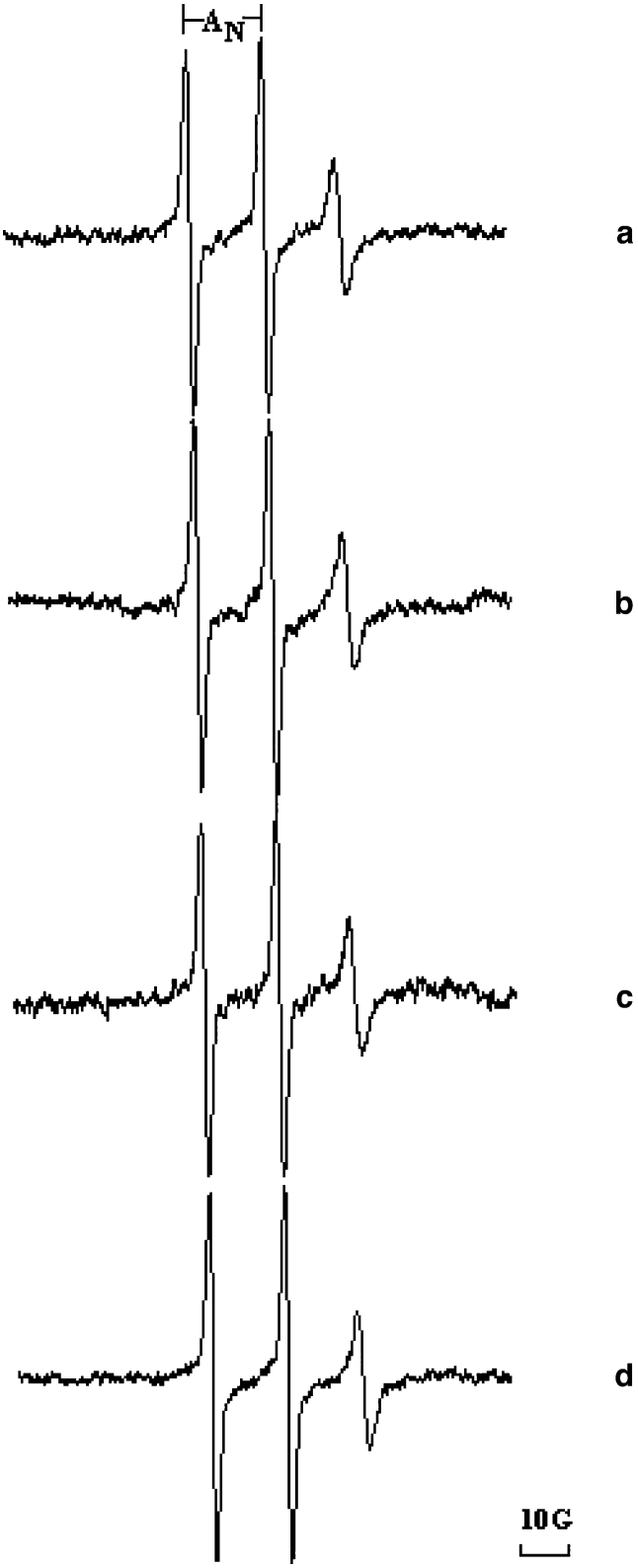

Fig. 7 ESR spectra of lamellar liquid crystal with different UV–irradiation time. The UV-irradiation time: a-2h, b-4h, c-6h, d-8h

References

1. Taulier N, Nicot C, Waks M, Hodges RS, Ober R, Urba W (2000) Biophys J 78:857
2. Chaudier Y, Zito F, Barthelemy P, Stroebel D, Ameduri B, Popot JL et al (2002) Bioorg Med Chem Lett 12:1587
3. Prata C, Giusti F, Gohon Y, Pucci B, Popot JL, Tribet C (2001) Biopolymers 56:77
4. Poulain FR, Nir S, Hawgood S (1996) Biochim Biophys Acta 169:1278
5. Guo YQ, Hui SW (1997) Biochim Biophys Acta 185:1323
6. Fendler JH (1982) Menbrane mimetic chemistry, Wiley, NewYork, pp 113-183
7. Lawrence MJ, Rees GD (2000) Adv Drug Deliver Rev 45:89
8. Uchegbu IF, Vyas SP (1998) Int J Pharm 172:33
9. Sadtler VM, Krafft MP, Riess JG (1999) Colloid Surf A 147:309
10. Vasudevan M, Wiencek JM (1997) J Colloid Interface Sci 186:185
11. Deo N, Jockusch S, Turro NJ, Somasundaran P (2003) Langmuir 19:5083
12. Ajloo D, Moosavi-Movahedi AA, Hakimelahi GH, Saboury AA, Gharibi H (2002) Colloid Surf B 26:185
13. Gelamo EL, Tabak M (2000) Spectrochim Acta A 56:2255
14. Moore PN, Puvvada S, Blankschtein D (2003) Langmuir 19:1009
15. Holmberg K (2001) Curr Opin Colloid Interface 6:148
16. Moran C, Clapes P, Comelles F, Garcia T, Perez L, Vinardell P, Mitjans M, Infante MR (2001) Langmuir 17:5071
17. Infante MR, Perez L, Pinazo A, Clapes P, Moran MC, Angelet M, Garcia MT, Vinardell MP (2004) C R Chem 7:583
18. Rodehuser L, Chaumetle H, Meyers A, Rogalska E, Gerardin C, Selve C (2000) Amino Acids 18:89
19. Vinardell P, Molinero J, Parra JL, Infante MR (1990) Int J Cosm Sci 12:13
20. Solans C, Pes MA, Azemar N, Infante MR (1990) Prog Colloid Polym Sci 81:144
21. Solans C, Azemar N, Infante MR, Warmheim T (1989) Prog Colloid Polym Sci 79:70
22. Jyothi AN, Sasikiran K, Nambisan B, Balagopalan C (2005) Process Biochem 40:3576
23. Tang YW (1999) Microcirculation Technique Magazine 9:49
24. Wang SH (1997) Modern Physical Knowledge 9:21
25. Dai WX, Yang YZ, Zhou RZ (1997) Cancer 17:29
26. Wei XC, Zhang ZZ (1994) Chinese Physical Therapy Magazine 17:39
27. Guo R, Zhang QQ, Qian JH, Zou AH (2002) Colloid Surf A 196:223
28. Liu TQ, Guo R (1996) J Dispers Sci Technol 17:509
29. Nokay ME, Ford LD, Fribery SE (1981) J Colloid Interface Sci 84:228
30. Sionkowska A, Wisniewski M, Skopinska J, Vicini S, Marsano E (2005) Polym Degrad Stab 88:261
31. Fobio CL, Chaimovich AH, Shirley S (1994) Langmuir 10:1786
32. Li F, Li GZ (1996) Chin J Chem Phys 9:527
33. Guo R, Liu TQ, Yu WL (1999) Langmuir 15:624
34. Bard J, Faulker LR (1980) Electrochemical Methods, New York, pp 234–239
35. Jahn W, Strey R (1988) J Phys Chem 92:2294